

# Absolute elastic electron-helium scattering cross-section measurements from 2 to 19 eV

D. E. Golden, J. Furst, and M. Mahgerefteh

*Department of Physics and Astronomy, University of Oklahoma, Norman, Oklahoma 73019*

(Received 30 March 1984)

Absolute  $e^-$ -He elastic differential scattering cross sections have been determined from relative scattered electron angular distribution measurements in the energy range from 2 to 19 eV. The absolute cross sections have been determined to within errors which vary from  $\pm 9\%$  to  $\pm 2\%$  within this energy range. The  $s$ ,  $p$ , and  $d$  phase shifts determined in this work are roughly in agreement with previous determinations, while the total and momentum-transfer cross sections determined in this work in some cases do not agree with previous determinations. The total and momentum-transfer cross sections found in this work at 2 and 5 eV are in excellent agreement with the previous direct measurements of Golden and Bandel and of Crompton *et al.*, respectively.

## I. INTRODUCTION

The elastic  $e^-$ -He scattering cross sections are the obvious experimental choices for standard cross sections against which other scattering cross sections can be calibrated. This is because He is a gas at room temperature which possesses no excited states below 19.8 eV, and calculations are relatively straightforward due to the fact that He is the simplest two-electron target.

The first absolute total  $e^-$ -He scattering cross-section measurements were reported by Ramsauer in 1921,<sup>1</sup> although in these and subsequent early measurements<sup>2,3</sup> no error estimates were given. Much more recently, absolute total cross-section measurements were performed by Golden and Bandel<sup>4</sup> for energies from 0.3 to 28 eV which were  $\sim 20\%$  lower than those of Ramsauer<sup>1</sup> and  $9\%$  lower than those of Ramsauer and Kollath.<sup>2</sup> These measurements had probable and maximum errors of  $\pm 3\%$  and  $\pm 7\%$ , respectively, mainly due to the absolute pressure measurement.

Momentum-transfer determinations were first placed on an absolute basis by Frost and Phelps.<sup>5</sup> This type of measurement was extended to higher energies and made more precise by Crompton *et al.*,<sup>6</sup> who have given maximum errors of  $\pm 2\%$  from 0.008 to 4.0 eV,  $3\%$  from 4.0 to 7.0 eV and  $\pm 5\%$  from 7 to 12 eV. Various procedures have been used by the above authors as well as others to determine momentum-transfer cross sections, from total cross-section measurements and *vice versa*. All of these efforts have led to the conclusion that agreement could only be established to about  $10\%$ .<sup>7</sup>

Of course, accurate differential cross-section measurements could be used to calculate both total and momentum-transfer cross sections. The first differential cross-section measurements were reported by Bullard and Massey in 1931,<sup>8</sup> but it was not until relatively recently that reliable differential cross sections have been measured. The reliability of differential cross-section measurements was greatly enhanced by the advent of two methods which did not require the absolute measurement of pressure to obtain absolute cross sections. One of these obtains absolute differential cross sections from the

analysis of a resonance profile while the other obtains absolute cross sections from the analysis of non-resonant angular distributions.

Analysis of the angular distribution at a resonance was first done by Andrick and Ehrhardt.<sup>9</sup> Later, Gibson and Dolder<sup>10</sup> deduced the  $S$ -,  $P$ -, and  $D$ -wave phase shifts from relative measurements of the 19.38-eV  $^2S$ -wave resonance. Their analysis was later corrected by Andrick<sup>11</sup> to include higher-order partial waves. Further measurements of this resonance were made by McConkey and Preston,<sup>12</sup> and Williams and Willis.<sup>13</sup> This work has been reviewed by Steph *et al.*,<sup>14</sup> who give the variations in  $\eta_0$ ,  $\eta_1$ ,  $\eta_2$ ,  $\sigma_T$ , and  $\sigma_{MT}$  as obtained by the above authors at 19.38 eV as about  $8\%$ ,  $4\%$ ,  $27\%$ ,  $11\%$ , and  $2\%$ , respectively.

The first complete phase-shift analysis of relative angular distribution measurements over a wide range of electron energies was done by Andrick and Bitsch.<sup>15</sup> These measurements and analysis allowed the determination of absolute elastic differential cross sections from 2 to 19 eV. Subsequently, the analysis was slightly corrected by Steph *et al.*<sup>14</sup> The errors associated with the absolute differential cross-section measurements at 2, 5, 12, and 19 eV as determined by Steph *et al.*<sup>14</sup> are  $52\%$ ,  $27\%$ ,  $10\%$ , and  $8\%$ , respectively. The results of this later analysis gives differential cross sections which deviate from those of previous direct absolute measurements<sup>12,16,17</sup> by as much as  $30\%$ .

Subsequently, absolute differential cross sections have been given by Register *et al.* in the energy range from 5 to 200 eV,<sup>18</sup> and by Williams<sup>19</sup> in the energy range from 0.5 to 20 eV. Both of these authors used methods of data analysis similar to that used by Steph *et al.*<sup>14</sup> to place relative differential cross-section measurements on an absolute scale. Both of these sets of measurements are in agreement with the results of Andrick and Bitsch.<sup>15</sup>

The best calculations available for elastic  $e^-$ -He scattering<sup>20-25</sup> yield  $S$ -wave phase shifts which agree with each other to about  $2\%$  or  $3\%$ , and  $P$ -wave phase shifts which agree with each other to about  $10\%$  or  $15\%$  while all higher-order phase shifts have been approximated by the Born approximation. These results give differential cross

sections which are in agreement with each other to within about 5% in the low-energy domain (2–20 eV) and also agree with the measurement of Register *et al.*<sup>18</sup> within the same amount.

We are interested in measuring accurate absolute low-energy electron-molecule differential scattering cross sections and have become interested in making more precise absolute elastic  $e^-$ -He differential scattering cross sections as a starting point for these other measurements. Therefore we have developed a pulsed-time-of-flight technique to make more precise measurements.

## II. EXPERIMENTAL APPARATUS AND PROCEDURE

A diagram showing the experimental arrangement is given in Fig. 1. The electron gun produces a pulsed beam of electrons which is crossfired with the atomic beam. The arrival time spectrum of scattered electrons is detected as a function of scattering angle while a signal proportional to the product of electron beam current and background gas density is monitored. The major advantage of the pulsed-time-of-flight-system in this work is its ability to distinguish between different flight paths at the same energy (different arrival times). This allows one to exclude electrons which have been reflected off various surfaces on their way to the detector (longer arrival times) from the measurement. This type of effect sometimes becomes significant ( $> 10\%$ ) in our apparatus for scattering angles larger than but near both  $0^\circ$  and  $90^\circ$ .

### A. Vacuum system

The apparatus is contained within a moly-permalloy magnetic shield inside the vacuum container which is itself enclosed within a set of Helmholtz coils. The magnetic field within the magnetic shield has been measured to be less than 0.3 mG. The main chamber is pumped by two trapped oil diffusion pumps and optionally by two titanium sublimation pumps. The atomic beam is optionally dumped into a turbomolecular pump. The atomic beam is skimmed and differentially pumped by another trapped oil diffusion pump.

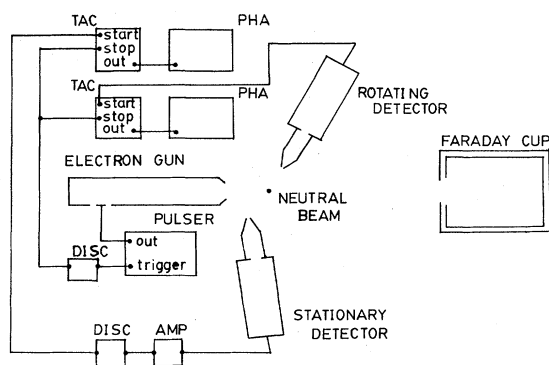


FIG. 1. The experimental arrangement.

### B. Electron gun

Electrons from an oxide-coated cathode or tungsten hairpin held in a Pierce configuration are focused through an aperture behind which a pulse is applied and then onto the atomic beam target. The electron gun produces a pulsed electron beam of about 0.25 eV full energy width at half intensity. The pulsed beam is produced by deflecting the electron beam past an aperture. The risetime of the electron current pulse may thus be diminished relative to the risetime of the pulse applied to the deflecting electrode. The pulse width is proportional to the rate of change of the pulse voltage and is adjustable. For the work reported here the pulse width used was about 50 nsec with a repetition rate of  $5 \mu$  sec. (However, pulse widths of the order of 50–100 psec have been achieved with this system.) In the present case ( $\sim 1\%$  duty cycle), the average current leaving the gun with the pulser on (as measured at the Faraday cup) was between  $5 \times 10^{-9}$  and  $3 \times 10^{-8}$  A.

A sample electron beam profile is shown in Fig. 2 where the current measured at a given angle is plotted versus scattering angle. The signals were obtained by measuring the current received by a grid in front of the rotating detector. In general it was relatively easy to obtain electron beam profiles with FWHM of about  $4^\circ$ . However, in order to be successful at measuring scattering cross sections of less than about  $40^\circ$  it was necessary to have an electron beam profile which dropped off by 4–5 orders of magnitude within  $10^\circ$ .

During the course of the work reported here, the electron gun was modified twice in order to decrease the width of the electron beam profile shown in Fig. 2. How-

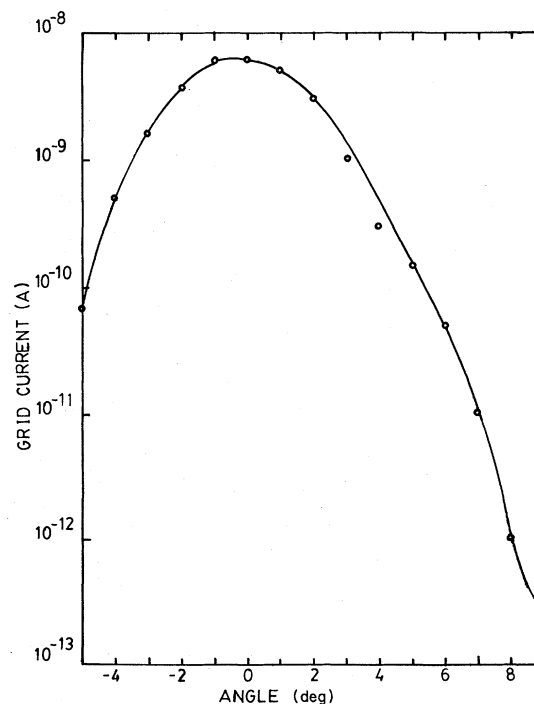


FIG. 2. Electron beam profile as viewed by the scattered-electron detector.

ever, while the width of this profile affected the lower angular limit to which scattering measurements could be made (in the best case  $10^\circ$ ), it did not noticeably affect the measured cross sections.

### C. Target beam source

In principle, the target beam source is relatively simple and has been described previously.<sup>26</sup> The gas is flowed through a 0.5-mm-diam tube with aspect ratio 100. The end of the tube is 0.5 mm from a 0.5-mm skimming aperture whose purpose is to cut the wings of the distribution emerging from the tube. The region below the skimming aperture is differentially pumped. The atomic beam arrangement described yields a beam to background density ratio of about 100 at the interaction region which is 5.0 mm above the differential pumping aperture. The capillary tube is driven by a large gas reservoir in which the pressure is monitored by an MKS Baratron gauge. The target gas density at the interaction region with the atomic beam on during the course of the work had an upper limit of approximately  $10^{12}/\text{cm}^3$ . In the course of a measurement, the atomic beam is turned off and the chamber flooded to the same background pressure as when the atomic beam is on. This is accomplished with two bypass valves so that the gas is not forced through the capillary tube.

### D. Scattered-electron detectors

As discussed above, two scattered-electron detectors are used to measure the scattered-electron signal and a signal proportional to the product of background pressure and electron beam current. The first has an acceptance solid angle of  $1.13 \times 10^{-2}$  sr and is rotatable from  $-60^\circ$  to  $+120^\circ$  with respect to the electron beam direction about the atomic beam axis while the second, which has an acceptance solid angle of  $1.77 \times 10^{-2}$  sr, is fixed and views a region along the electron beam between the output snout of the electron gun and the atomic beam. Both detectors consist of a pair of channel plates preceded by a pair of grids and followed by a metal output plate.

### E. Energy calibration

Two methods of energy calibration were used in this work. One method was to measure the energy position of the lowest  $^2S$  resonance,<sup>27</sup> as determined from the voltage between the cathode and interaction region. The other was to measure the retarding potential necessary to prevent scattered electrons from reaching the rotating detector at a particular accelerating voltage. The voltage position of the maximum of the measured energy distribution function was taken to be the electron energy. These two procedures gave agreement at the position of the  $^2S$  resonance to be about 0.05 eV. We would expect the energy scale to be good to about 0.1 eV at all energies.

### F. Relative cross-section measurements

The absolute cross-section measurements reported in this work have been determined by measuring a

scattered-electron signal rate from the atomic beam as a function of scattering angle using the rotating detector,  $\dot{R}(E, \theta)$ , as well as a scattered-electron signal rate from the background gas at each scattering angle used using the stationary detector,  $\dot{S}(E, \theta)$ . In addition, signal rates from both detectors were also measured with the atomic beam off and the chamber flooded to the same background pressure as when the atomic beam was on,  $\dot{R}'(E, \theta)$  and  $\dot{S}'(E, \theta)$ , respectively. The relative differential cross section at a particular electron energy  $E$  for scattering angles  $\theta$  is determined from the following equation:

$$\sigma(E, \theta) = \frac{\dot{R}(E, \theta)}{\dot{S}(E, \theta)} - \frac{\dot{R}'(E, \theta)}{\dot{S}'(E, \theta)}. \quad (1)$$

Pulses from the rotating and fixed electron detectors were used to start two time-to-amplitude converters (TAC) which were both stopped by a pulse derived from that which triggered the electron gun pulse. Each TAC was pulse-height analyzed and the resulting arrival time spectra stored. A sample time spectra from the rotating detector is shown in Fig. 3. The measurements were made for various driving pressures and were found to be independent of the driving pressure for pressures between about 3 to 20 Torr (which corresponds to a background gas pressure range of about  $1.5 \times 10^{-7}$  to about  $1 \times 10^{-6}$  Torr in the chamber).

The justification for Eq. (1) with  $\dot{S}$  and  $\dot{S}' = 1$  has been given by Andrick and Bitsch.<sup>15</sup> Here a treatment using a notation similar to that of Steph *et al.*<sup>14</sup> will be given. When the atom beam is off, the scattered-electron signal rate at the rotating detector is given by

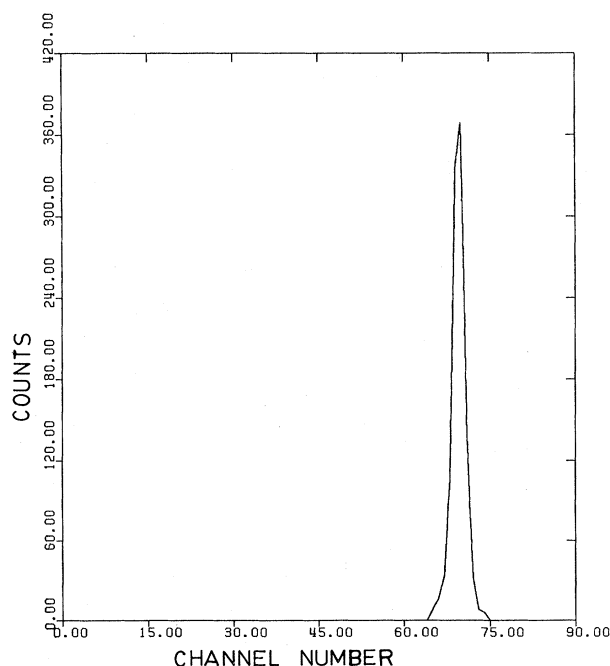


FIG. 3. A sample 10-sec time spectrum from the rotating detector for scattering at  $90^\circ$ . (Time scale increases from right to left.)

$$\dot{R}'(E, \theta) = \frac{I_e}{e} \rho_0 \epsilon_R \sigma(E, \theta) L_e, \quad (2)$$

where  $I_e/e$  is the number of incident electrons per second in the electron beam,  $\rho_0$  is the background gas density,  $\epsilon_R$  is the efficiency of the rotating electron detector, and

$$L_e = \int_{\Delta\Omega_e} \int_{l_e} d\Omega dz \quad (3)$$

is the average path length viewed by the rotating detector. If the atom beam has a density  $\rho_B$  which is sharply defined, we may write

$$\frac{\rho}{\rho_0} = \frac{\rho_B}{\rho_0} + 1, \quad (4)$$

where  $\rho$  is the target density when the atom beam is on. Then, when the atom beam is on, the scattered-electron signal rate at the rotating detector is given by

$$\dot{R}(E, \theta) = \frac{I_e}{e} \rho_0 \epsilon_R \sigma(\epsilon, \theta) \left[ \int_{\Delta\Omega_e} \int_{l_e} \frac{\rho_B}{\rho_0} d\Omega dz + L_e \right]. \quad (5)$$

The stationary detector views scattering from the background gas whether or not the atom beam is on. Therefore, the signal rates to the stationary detector with the beam on and off, are both given by

$$\dot{S}(E, \theta) = \dot{S}'(E, \theta) = \frac{I_e}{e} \rho_0 \epsilon_s \int_{\Delta\Omega_e} \int_{l_e} \sigma(E, \theta) d\Omega dz. \quad (6)$$

That is, in either case we have a signal proportional to the product of electron beam current and background gas density. (The integral is a constant.)

Thus, the signals given by Eq. (6) can be used to normalize the signals given by Eq. (2) and Eq. (5) and properly account for fluctuations in the electron and atomic beam signal intensities. Subtracting the normalized signal derived from Eq. (2) and Eq. (5) one obtains

$$\frac{\dot{R}(E, \theta)}{\dot{S}(E, \theta)} - \frac{\dot{R}'(E, \theta)}{\dot{S}'(E, \theta)} = \sigma(E, \theta) \left( \frac{\epsilon_R}{\epsilon_s} \right) \frac{\int_{\Delta\Omega_e} \int_{l_e} \frac{\rho_B}{\rho_0} d\Omega dz}{\int_{\Delta\Omega_e} \int_{l_e} \sigma(E, \theta) d\Omega dz} \quad (7)$$

which is a signal proportional to the differential cross section provided that the ratio of detection efficiencies and the geometrical factors in Eq. (7) remain constant. Thus Eq. (1) may be used to measure relative differential cross sections. The measurements were made from  $115^\circ$  to the smallest angle used in  $10^\circ$  steps and then by returning to large angles in  $10^\circ$  steps offset by  $5^\circ$ . This usually resulted in about 20 points.

### G. Absolute cross-section determinations

The procedure used to determine absolute cross sections from relative cross-section measurements has been given in detail by Steph *et al.*,<sup>14</sup> and will only be outlined here. The measured relative differential cross sections (DCS) are fitted to an analytic phase-shift expansion representation of the DCS where the first several phase shifts are as-

sumed to be unknowns and the rest are represented by the Born sum:

$$\sigma(\theta, E) = \frac{1}{4E} \left[ \left[ \sum_{l=0}^L (2l+1) \sin(2\eta_l P_l + 2\sqrt{E} f_B^L) \right]^2 + \left[ \sum_{l=0}^L (2l+1) [\cos(2\eta_l) - 1] P_l \right]^2 \right], \quad (8)$$

where  $\eta_l$  is the phase shift of the  $l$ th partial wave,  $P_l$  is the  $l$ th Legendre polynomial,  $f_B^L$  is the sum of the remaining Born amplitudes given by

$$f_B^L = \pi\alpha\sqrt{E} \left[ \frac{1}{3} - \frac{1}{2} \sin\left(\frac{1}{2}\theta\right) - \sum_{l=1}^L \frac{P_l}{(2l+3)(2l-1)} \right], \quad (9)$$

and the  $\eta_l$  from 0 to  $L$  are used as unknown parameters in the fitting procedure. Throughout the course of this work  $L=2$ .

The best fit to the data was determined as that fit which gave a minimum reduced chi square  $\chi^2$  defined by

$$\chi^2 = \frac{1}{N-P} \sum_{\theta_i} \left[ \frac{\kappa^{-1} \sigma_c(\theta_i) - \sigma_m(\theta_i)}{\Delta\sigma_m(\theta_i)} \right]^2, \quad (10)$$

where  $N$  is the number of angles and  $P$  the number of parameters ( $P=4$  in this work),  $\sigma_c$  and  $\sigma_m$  the calculated and measured DCS,  $\Delta\sigma_m$  is the fractional error in  $\sigma_m$ , and  $\kappa$  is the scale factor for the relative DCS.

Once the DCS are determined, the total cross section  $\sigma_T$  and the momentum-transfer cross section  $\sigma_{MT}$  may be calculated,

$$\sigma_T = \frac{4\pi}{E} \sum_{l=0}^{\infty} (2l+1) \sin^2 \eta_l, \quad (11)$$

$$\sigma_{MT} = \frac{4\pi}{E} \sum_{l=0}^{\infty} (l+1) \sin^2(\eta_l - \eta_{l+1}). \quad (12)$$

It should be noted that the scale factors for relative differential cross sections, measured at different energies, are not independent of each other. Rather, they are related through the measured signals at the different energies. This then allows the measurements to be extended upwards in energy although the type of phase-shift analysis described here is only valid for energies below the threshold of the first excited state.

### H. Error analysis

Since the equation used in the fitting of the DCS is nonlinear in the fitting parameters one needs to define a reasonable criterion from which to obtain the errors. In this work, all combinations of the first three phase shifts which resulted in curves lying within 5% of all but two data points were accepted. The errors in all parameters were determined as the range of the parameters in the accepted fits.

## III. RESULTS

Samples of the differential cross-section measurements made according to the procedure discussed above are

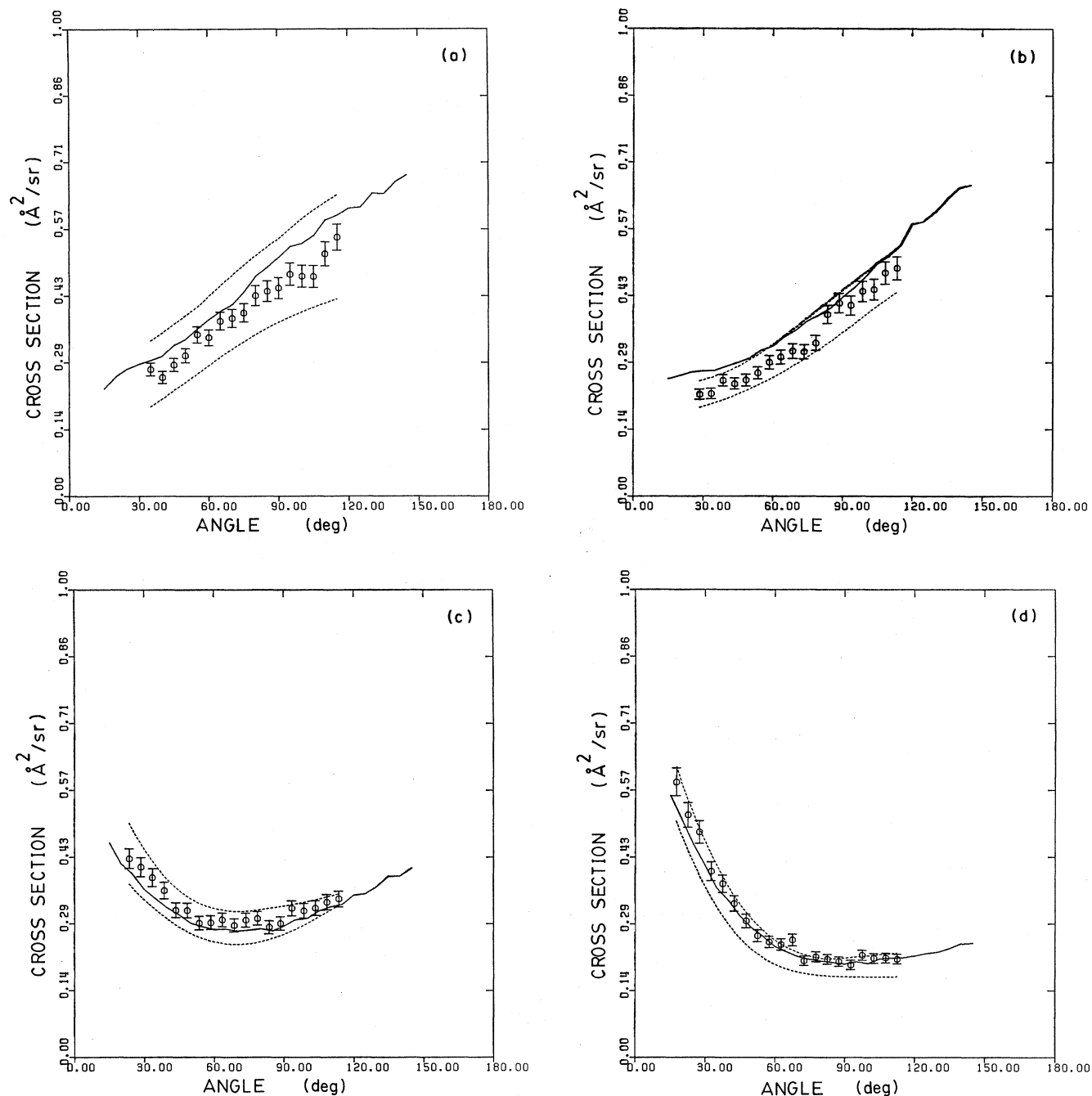


FIG. 4. Sample differential cross-section measurements at (a) 2 eV (b) 5 eV, (c) 12 eV, and (d) 19 eV. Data are at the level determined as the "best fit" to the data while the dashed lines are the limits of the scale as determined in this work. Solid line is the data of Andrick and Bitsch (Ref. 15) placed at the level determined in this work.

shown in Fig. 4 at 2, 5, 12, and 19 eV. The scales on the figures have been determined by the fitting procedure also described above while the two dashed lines on each figure are the limits of the scale as determined in this work. The solid line on each figure is the data of Andrick and Bitsch<sup>15</sup> at the level given by them as the best fit to their data.

The first three phase shifts as determined in this work are presented in Table I along with those determined in

previous measurements and calculations. The present results are the result of weighted averages of different runs made over a long period of time. At each energy at least four runs have been made. The errors given have been determined by combining the statistical errors of all the data used. The differential cross section scale has been determined to have errors of  $\pm 9\%$ ,  $+ 8.3\% - 7.1\%$ ,  $+ 8.0\% - 6.0\%$ , and  $+ 1.9\% - 2.1\%$  at 2, 5, 12, and 19 eV, respectively. This is to be compared to an error which

TABLE I. The first three phase shifts in radians.

Energy (eV)	$\eta_0$	$\eta_1$	$\eta_2$	Author
2	2.65(+0.9% -0.9%)	0.046(+13.5% -13.5%)	0.008(+27.0% -27.0%)	Present
	2.62(+5.0% -5.0%)	0.052(+37.0% -37.0%)	0.006 (fixed)	Andrick and Bitsch <sup>a</sup>
	2.52(+1.8% -1.8%)	0.066(+24.9% -18.9%)	0.009(+63.0% -62.0%)	Andrick and Bitsch <sup>b</sup>
	2.61(+2% -2%)	0.060(+2.0% -2.0%)	0.006(+8.0% -8.0%)	Williams <sup>c</sup>
	2.62	0.046	0.006 (fixed)	O'Malley <i>et al.</i> <sup>d</sup>
	2.64	0.056	0.006 (fixed)	Nesbet <sup>e</sup>
5	2.39(+1.1% -1.3%)	0.114(+8.6% -10.8%)	0.016(+52.0% -53.0%)	Present
	2.32(+2.0% -2.0%)	0.135(+19.0% -19.0%)	0.015 (fixed)	Andrick and Bitsch <sup>a</sup>
	2.34(+2.0% -2.0%)	0.126(+25.0% -25.0%)	0.010(+108.0% -108.0%)	Andrick and Bitsch <sup>b</sup>
	2.35(+10.0% -3.6%)	0.118(+44.0% -50.0%)	0.011(+108.0% -108.0%)	Register <i>et al.</i> <sup>b,e</sup>
	2.32(+2% -2%)	0.129(+2% -2%)	0.014(+8% -8%)	Williams <sup>c</sup>
	2.33	0.114	0.015 (fixed)	O'Malley <i>et al.</i> <sup>d</sup>
12	2.34	0.124	0.015 (fixed)	Nesbet <sup>e</sup>
	2.01(+0.5% -3.2%)	0.250(+0.9% -7.9%)	0.037(+19.7% -19.4%)	Present
	1.99(+3.0% -3.0%)	0.259(+12.0% -12.0%)	0.037 (fixed)	Andrick and Bitsch <sup>a</sup>
	1.99(+2.6% -2.6%)	0.255(+9.0% -9.0%)	0.036(+36.0% -36.0%)	Andrick and Bitsch <sup>b</sup>
	1.96(+3.6% -4.8%)	0.272(+12.0% -16.2%)	0.036(+45.0% -45.0%)	Register <i>et al.</i> <sup>c,e</sup>
	1.97(+1.9% -1.9%)	0.242(+2.0% -2.0%)	0.037(+8.0% -8.0%)	Williams <sup>c</sup>
19	1.98	0.236	0.037 (fixed)	O'Malley <i>et al.</i> <sup>d</sup>
	1.99	0.243	0.037 (fixed)	Nesbet <sup>e</sup>
	1.84(+1.9% -2.0%)	0.353(+3.2% -4.3%)	0.065(+12.9% -10.8%)	Present
	1.81(+5% -5%)	0.325(+12% -12%)	0.058 (fixed)	Andrick and Bitsch <sup>a</sup>
	1.82(+4.2% -3.4%)	0.325(+11.0% -11.2%)	0.060(+27.0% -22.0%)	Andrick and Bitsch <sup>b</sup>
	1.82(+1.5% -1.5%)	0.305(+2% -2%)	0.056(+8% -8%)	Williams <sup>c</sup>
1.80	0.316	0.058 (fixed)	Nesbet <sup>e</sup>	

<sup>a</sup>Reference 15.<sup>b</sup>Present analysis.<sup>c</sup>Reference 13.<sup>d</sup>Reference 25.<sup>e</sup>Reference 24.<sup>f</sup>Reference 18.

decreases from  $\pm 20\%$  to  $\pm 5\%$  in this energy range given by Andrick and Bitsch,<sup>15</sup>  $\pm 5\%$  in this energy range given by Register *et al.*,<sup>18</sup> and  $\pm 4\%$  given by Williams at 19.2 eV.<sup>19</sup>

The phase shifts as determined in this work are in general agreement within the errors with the result of the previous measurements of Andrick and Bitsch,<sup>15</sup> Register *et al.*,<sup>18</sup> and Williams,<sup>19</sup> as well as the calculations of Nes-

TABLE II. Total cross section in  $\text{\AA}^2$ .

Energy (eV)	2	5	12	19
Present	5.58(+9.7% -8.9%)	4.89(+4.5% -7.5%)	4.24(+2.1% -3.2%)	3.12(+0.6% -2.1%)
Andrick and Bitsch <sup>a</sup>	6.20(+50.0% -50.0%)	5.64(+11.0% -11.0%)	4.15(+4.0% -4.0%)	3.19(+4.0% -4.0%)
Andrick and Bitsch <sup>b</sup>	8.47(+14.4% -13.3%)	5.41(+11.7% -11.2%)	4.11(+3.4% -3.5%)	3.19(+3.5% -3.4%)
Register <i>et al.</i> <sup>c</sup>		5.25(+3% -3%)	3.96(+3% -3%)	
Register <i>et al.</i> <sup>b</sup>		5.26(+19.9% -47.1%)	4.31(+4.5% -4.1%)	
Golden and Bandel <sup>d</sup>	5.57(+7% -7%)	4.95(+7% -7%)	3.70(+7% -7%)	2.87(+7% -7%)
Kennerly and Bonham <sup>e</sup>	6.01(+3% -2%)	5.25(+3% -2%)	3.96(+3% -2%)	3.11(+3% -2%)
O'Malley <i>et al.</i> <sup>f</sup>	6.00	5.58	4.25	
Nesbet <sup>g</sup>	6.03	5.38	4.06	3.13

<sup>a</sup>Reference 15.<sup>b</sup>Present analysis.<sup>c</sup>Reference 18.<sup>d</sup>Reference 4.<sup>e</sup>Reference 29.<sup>f</sup>Reference 25.<sup>g</sup>Reference 24.

TABLE III. Momentum-transfer cross section in  $\text{\AA}^2$ .

Energy (eV)	2	5	12	19
Present	6.43(+10.7% -9.8%)	5.84(+5.1% -7.7%)	4.33(+0.8% -2.7%)	2.92(+1.8% -3.7%)
Andrick and Bitsch <sup>a</sup>	7.20(+40.0% -40.0%)	6.64(+11% -11%)	4.28(+3% -3%)	2.86(+4% -4%)
Andrick and Bitsch <sup>b</sup>	9.84(+15.8% -14.3%)	6.40(+11.8% -11.7%)	4.26(+2.7% -2.9%)	2.86(+3.4% -3.4%)
Register <i>et al.</i> <sup>c</sup>		6.45(+3% -3%)	4.27(+5% -5%)	
Register <i>et al.</i> <sup>b</sup>		6.20(+18.0% -47.4%)	4.39(+3.4% -3.4%)	
Crompton <i>et al.</i> <sup>d</sup>	6.98(+2% -2%)	6.31(+3% -3%)	4.15(+5% -5%)	
O'Malley <i>et al.</i> <sup>e</sup>	6.88	6.52	4.53	
Nesbet <sup>f</sup>	7.00	6.32	4.21	2.85

<sup>a</sup>Reference 15.<sup>b</sup>Our analysis.<sup>c</sup>Reference 18.<sup>d</sup>Reference 6.<sup>e</sup>Reference 25.<sup>f</sup>Reference 24.

bet<sup>24</sup> and O'Malley *et al.*<sup>25</sup> However, the *p*-wave phase shifts determined in this work are slightly outside of the error-bar overlap with those of Williams<sup>19</sup> and Nesbet<sup>24</sup> at 2, 5, and 19 eV. It should also be noted that the present analysis of the experimental results of Andrick and Bitsch<sup>15</sup> and Register *et al.*<sup>18</sup> yields lower  $\chi^2$  than given by those authors.

The resulting total and momentum-transfer cross sections are tabulated in Tables II and III, respectively. The present result for the total cross section at 2 eV is in excellent agreement with the previous result of Golden and Bandel.<sup>4,28</sup> It agrees with the previous result given by Andrick and Bitsch<sup>15</sup> although it is near the end of the error bar. However, the present result drastically disagrees with the present analysis of the 2-eV data of Andrick and Bitsch. The present results also agree with the previous results of Nesbet,<sup>24</sup> O'Malley *et al.*,<sup>25</sup> and Kennerly and Bonham,<sup>29</sup> although in all of these cases the agreement is at or near the end of the present error bar. The present result for the total cross section at 5 eV is also in excellent agreement with the previous result of Golden and Bandel.<sup>4</sup> In this case the result disagrees with that of Andrick and Bitsch,<sup>15</sup> Nesbet,<sup>24</sup> and O'Malley *et al.*,<sup>25</sup> while it is just at the end of the overlap of error bars with Register

*et al.*<sup>18</sup> and just outside of error-bar overlays with Kennerly and Bonham.<sup>29</sup> At 12 eV the present total cross-section result is several percent outside of the overlap of error bars with the previous result of Golden and Bandel<sup>4</sup> and it is in better agreement with the previous results of Andrick and Bitsch.<sup>15</sup> It is just outside of error overlap with Register *et al.*<sup>18</sup> and Nesbet.<sup>24</sup> The present total cross-section result at 19 eV is in agreement with the previous result of Golden and Bandel,<sup>4</sup> although it is in better agreement with the previous results of the other measurements and calculations.

The present results for the momentum-transfer cross sections are below the previous results at 2 and 5 eV, are about the same at 12 eV, and are slightly above the previous results at 19 eV. The present momentum-transfer cross-section results are in agreement with past results within the respective errors except for the results of Nesbet<sup>24</sup> and O'Malley *et al.*<sup>25</sup> at 5 and 12 eV. In all cases these results are very close to error-bar overlap.

#### ACKNOWLEDGMENT

This work was supported by the Office of Basic Energy Sciences, U. S. Department of Energy.

<sup>1</sup>C. Ramsauer, Ann. Phys. (Leipzig) **64**, 513 (1921).<sup>2</sup>C. Ramsauer and R. Kollath, Ann. Phys. (Leipzig) **3**, 536 (1929); **10**, 143 (1931); **12**, 529 (1932).<sup>3</sup>C. E. Normand, Phys. Rev. **35**, 1217 (1930).<sup>4</sup>D. E. Golden and H. W. Bandel, Phys. Rev. **138**, A14 (1965).<sup>5</sup>L. S. Frost and A. V. Phelps., Phys. Rev. **136**, A1538 (1964).<sup>6</sup>See, for example, R. W. Crompton, M. T. Elford, and A. G. Robertson, Aust. J. Phys. **23**, 667 (1970); H. B. Milloy and R. W. Crompton, Phys. Rev. A **15**, 1847 (1977).<sup>7</sup>See, for example, B. Bederson and L. J. Kieffer, Rev. Mod. Phys. **43**, 601 (1971).<sup>8</sup>E. C. Bullard and H. S. W. Massey, Proc. R. Soc. London, Ser. A **133**, 637 (1931).<sup>9</sup>D. Andrick and H. Ehrhardt, Z. Phys. **192**, 99 (1966).<sup>10</sup>J. R. Gibson and K. T. Dolder, J. Phys. B **2**, 741 (1968).<sup>11</sup>D. Andrick, Adv. At. Mol. Phys. **9**, 207 (1973).<sup>12</sup>J. W. McConkey and J. A. Preston, J. Phys. B **8**, 63 (1975).<sup>13</sup>J. F. Williams and B. A. Willis, J. Phys. B **8**, 1641 (1975); **8**, 1670 (1975).<sup>14</sup>N. C. Steph, L. McDonald, and D. E. Golden, J. Phys. B **12**, 1507 (1979).<sup>15</sup>D. Andrick and A. Bitsch, J. Phys. B **8**, 393 (1975).<sup>16</sup>J. R. Gibson and K. T. Dolder, J. Phys. B **2**, 1180 (1969).<sup>17</sup>S. K. Srivastava and S. Trajmar, J. Chem. Phys. **64**, 3886 (1976).<sup>18</sup>D. F. Register, S. Trajmar, and S. K. Srivastava, Phys. Rev. A **21**, 1134 (1980).<sup>19</sup>J. F. Williams, J. Phys. B **12**, 265 (1979).<sup>20</sup>W. M. Duxler, R. T. Poe, and B. A. LaBahn, Phys. Rev. A **4**, 1935 (1971).<sup>21</sup>A. L. Sinfailam and R. K. Nesbet, Phys. Rev. A **6**, 2118 (1972).

<sup>22</sup>B. S. Yarlagadda, G. Csanak, H. S. Taylor, B. Schneider, and R. Yaris, *Phys. Rev. A* **7**, 146 (1973).

<sup>23</sup>E. Wichmann and P. Heiss, *J. Phys. B* **7**, 1042 (1974).

<sup>24</sup>R. K. Nesbet, *Phys. Rev. A* **20**, 50 (1979).

<sup>25</sup>T. F. O'Malley, P. G. Burke, and K. A. Berrington, *J. Phys. B* **12**, 953 (1979).

<sup>26</sup>V. C. Sutcliffe, G. N. Haddad, N. C. Steph, and D. E. Golden, *Phys. Rev. A* **17**, 100 (1978).

<sup>27</sup>For a discussion of the energy position of this resonance see,

for example, D. E. Golden, *Adv. At. Mol. Phys.* **14**, 1 (1978).

<sup>28</sup>It should be noted that when the rotating detector discriminator was adjusted too low to completely eliminate the noise present, the effect at 2 eV was to flatten the measured angular distribution so that it gave results similar to those of Andrick and Bitsch.

<sup>29</sup>R. E. Kennerly and R. A. Bonham, *Phys. Rev.* **17**, 1844 (1978).